Evaluation of solar thermal pretreatment of carbonate-rich manganese ores in high-carbon ferromanganese production through dynamic process modelling

by L. Hockaday[1,2], F. Dinter[2], Q.G. Reynolds[3,4], and C. McGregor[2]

Affiliation:
[1]Curtin University, Western Australia School of Mines, Kent Street, Bentley, WA, Australia
[2]Stellenbosch University, Department of Mechanical and Mechatronic Engineering, Stellenbosch, South Africa
[3]Stellenbosch University, Department of Process Engineering, Stellenbosch, South Africa
[4]Mintek, Pyrometallurgy Division, 200 Malibongwe Drive, Randburg, South Africa

Correspondence to:
L.Hockaday

Email:
lina.hockaday@curtin.edu.au

Dates:
Received: 18 Feb. 2024
Revised: 14 Sept. 2024
Accepted: Nov. 20241
Published: December 2024

How to cite:
Hockaday, L., Dinter, F., Reynolds, Q.G., and MaGregor, C. 2024. Evaluation of solar thermal pretreatment of carbonate-rich manganese ores in high-carbon ferromanganese production through dynamic process modelling. *Journal of the Southern African Institute of Mining and Metallurgy*, vol. 124, no.12 pp. 763–776

DOI:
http://dx.doi.org/10.17159/2411-9717/3296/2024

ORCiD:
L. Hockaday
http://orcid.org/0000-0003-2597-9756

Abstract

The necessity of reducing greenhouse gas emissions to limit the impact of anthropogenic climate change means that all industrial processes should investigate their options towards decarbonization. Iron, steelmaking, aluminium, and cement production produce the most industrial emissions. Although most research focuses on decarbonizing these industries, minerals processing industries must be decarbonized to achieve net zero emissions goals by 2050. Incorporating renewable energy sources and avoiding the combustion of fossil fuels are two ways to reduce greenhouse gas emissions. This paper reports on the results from a dynamic process model developed to investigate the feasibility of concentrating solar thermal pretreatment of manganese ores to pretreat carbonate-rich manganese ores for increased ferromanganese smelter productivity and reduced greenhouse gas emissions. The results indicate that pretreated ores reduce the energy requirement for smelting significantly for some ores and lowers total carbon dioxide emissions by 13 to 19% compared to the traditional smelting route. A high-level economic evaluation shows that solar thermal treatment is financially viable for low cryptomelane, high braunite ore that is common in the Kalahari Manganese Field.

Keywords

solar thermal, manganese ore, dynamic modelling, benefit assessment

Introduction

Globally, pressure has mounted on the mining and minerals processing sector to show commitment to fighting climate change by enacting sustainable governmental practices – one of which is lowering greenhouse gas (GHG) emissions. Concerns about the emission of GHG and their contribution to climate change have led to South Africa implementing a carbon tax on carbon dioxide emissions (South African Government, 2019). Despite the carbon tax having been introduced with large emission allowances, it is generally accepted that these allowances will be reduced over time to align with European regulations. Awareness of the impact of climate change has become more prevalent and having a social license to operate has become crucial in metal production (International Resource Panel, 2020; Mills, 2021).

This paper aims to investigate concentrating solar thermal pretreatment of manganese ores for ferroalloy production. This technology can be seen as a process energy efficiency initiative for smelters, replacing fossil fuel and reductant with solar energy. The use of carbon capture and sequestration of carbon dioxide emissions emitted during solar thermal pretreatment may be investigated in future but fall outside the scope of this study.

Current manganese ore pretreatment technologies (Olsen, Tangstad and Lindstad, 2007; Gasik, 2013; Gordon Y., 2013; Gordon, Nell and Yaroshenko, 2018) may be classified as preheating, calcination or sintering. Preheated materials are charged directly to smelters at 600–700°C after heating in rotary kilns with coal or furnace off-gas combustion and lower electric energy consumption by more than 20% (Tanabe, 1968; Ishak and Tangstad, 2007; Tangstad, Ichihara and Ringdalen, 2015). The calcination of manganese ores is mainly used as a preparation step for electrolytic processes in the production of high-purity manganese metal and manganese dioxide. Manganese ores mixed with ground coal are heated at temperatures between 850°C and 900°C to achieve the reduction of manganese to Mn^{2+} as well as carbonate decomposition (Harris, Meyer and Auerswald, 1977; Biswal et al., 2015). Sintering of manganese ores mixed with coal occurs at temperatures above 1200°C, decomposing all carbonates and reducing manganese oxides to MnO. Sinter operations are well described in the literature (Gericke, 1989; Pienaar and Smith, 1992; Daavittila et al., 2001; Malan, Barthel and Dippenaar, 2004; Zhang et al., 2013).

Table I

Reaction rate equations and activation energies and pre-exponential factors determined from experimental data (Hockaday, Dinter and Reynolds, In print)

Reaction	Rate equation	E_a, kJ/mol	A
$CaMg(CO_3)_2 \rightarrow CaO + MgO + 2CO_2(g)$	$1 - (1 - X_i)½$	175–190	4368805 4368805
$MgCO_3 \rightarrow MgO + CO_2$ (g)	0.6% for 100 °C < T < 400 °C $1 - (1 - X_i)$ ½ for T > 400 °C	165	4368805
$4MnO_2 \rightarrow 2Mn_2O_3 + O_2(g)$ $6Mn_2O_3 \rightarrow 4Mn_3O_4 + O_2(g)$	$1 - (1 - X_i)⅓$	62.6 65.5	23426100 4072865
Reduction reactions with solid carbon	$1 - (1 - X_i)⅓$	18.0	0.00038

Pretreatment of manganese ores is currently practised only in reducing atmospheres. A novel concentrating solar thermal pretreatment in air has been proposed to offer the advantages of carbonate decomposition while limiting the reduction of manganese oxides to Mn_3O_4 (Hockaday, Dinter and Reynolds, In print). Materials treatment with concentrating solar technologies is still a developing field of research, but much progress has been made in the last decade (Ekman, Brooks and Rhamdhani, 2014; Koepf et al., 2017). Solar particle reactor technology has been researched for various applications, including solar processing of composite iron ore pellets (Purohit et al., 2018), particles as a heat transfer medium (Amsbeck et al., 2014), and the calcination of lime (Flamant et al., 2018). Several desktop studies have also been published regarding indirect solar heating in fuel-saving applications for manganese ore pretreatment (Hockaday, Dinter and Harms, 2018; Lubkoll, Hockaday and Harms, 2018). Desktop studies for indirect solar preheating of manganese ores up to 600°C using air as heat transfer medium and including thermal storage have also been shown as more cost effective that electrification of preheating (Hockaday et al., 2020; Mckechnie, McGregor and Venter, 2020, 2022).

The current study focuses on direct solar heating of manganese ores in air as a pretreatment for high-carbon ferromanganese production. The direct solar treatment of manganese ores has been performed on small scale and showed promising decomposition of carbonate minerals (Hockaday et al., 2021). The scaling of direct solar thermal treatment of manganese ores was evaluated based on several models describing the solar resource, the manganese ore reaction kinetics, and a solar particle reactor. These models were linked in HSC SIM (Roine and Bjorklund, 2002; Outotec, 2019) to estimate the annual production and composition of solar thermal pretreated manganese ores. The energy demand of solar-treated material in a high-carbon ferromanganese furnace was then investigated based on an HSC Sim distribution model.

Theory

The reduction and calcination reactions that occur in high-calcite manganese ore pretreatment have been described by Hockaday, Dinter and Reynolds (In print). Thermal treatment in non-reducing conditions allows the decomposition of carbonate minerals, pyrolusite and bixbyite decomposed to hausmannite, and partial decomposition of braunite to hausmannite. The kinetic models describing the ore behaviour are summarized in Table I.

Mass and energy balances

Mass and energy balances were performed with HSC SIM software. The reactor energy balance was based on the solar energy entering the reactor being split between three reactor zones: Tank 1, Tank 2, and Tank 3. Each tank was assumed to act as an ideal mixer or continuously stirred tank reactor (CSTR), with all materials inside reaching the same temperature. The flows of gas and solid materials were counter-current. Tank 1 received untreated materials and served as an outlet for the process off-gas. Tank 3 received the solar flux and an air inflow and served as the kiln discharge for treated materials. The stream flows and operations of the dynamic process model are shown in Figure 1.

Control philosophy for the solar plant

The control philosophies, and calculations for each time step, are described below:

- The receiver was charged with a batch of material to protect the receiver from solar flux. The batch size may vary from 120 kg to 500 kg based on the material density.

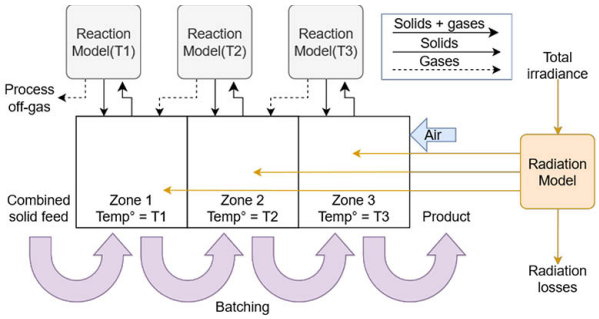

Figure 1—Stream flows and operations in the dynamic process model

- Feed material was added to Tank 1 based on the feed rate setpoint if the temperatures in the receiver were high enough. For solar irradiance levels below 1000 kW the feed rate setpoint was halved.
- The solar irradiance was taken from the dynamic SET sheet and used in the radiation model, together with the current temperatures of the tanks, to determine the irradiance into each tank and the radiation losses from the receiver.
- An energy balance was performed on each tank based on the energy flows determined in the previous step to determine the new temperature of each zone.
- Materials in each tank were converted according to the reaction rate model and used to calculate the new composition of the tank. Product gasses flow to the previous tank number counter-current to the flow of solid materials.
- Solid materials were batched to the next tank or discharged to the product pile if the tank was too full.
- When the discharge zone temperature dropped below 950°C the addition of feed material was stopped. The receiver discharged until it reached the maximum capacity and then held the rest of the material inside the receiver. The mass and energy balances, and the reaction rate model, were still applied.

Assumptions for the dimensions and operation of the receiver are based on published data of the CentRec® receiver (Ebert et al., 2016, 2018, 2019; Amsbeck et al., 2018) and are given in Table II. The CentRec® demonstration unit was tested with ceramic particles of 1 mm diameter. Similar behaviour was assumed for manganese ore particles. Manganese ore fines (< 6 mm) are readily available for processing at mines and smelters and are currently treated as waste or agglomerated through sintering or briquetting (Olsen, Tangstad and Lindstad, 2007), and can be the source for manganese ore particles of approximately 1 mm.

When the particle volume in the tank exceeds the maximum volume calculated for the layer thickness, particles in the tank are batched to the next tank or discharged, depending on the tank number. The dynamic module automatically calculates the volume of the solids in each tank, based on density values contained in the thermodynamic database. Each tank was specified to run in the energy input mode in the simulation, where the energy balance was solved to determine the new temperature of the tank at the end of each timestep.

A crucial aspect of the receiver is its ability to hold the particles in the receiver at high rotational speeds and then discharge the particles by reducing rotational speed. This enables fine control over the temperature of the discharge material. The feed material control temperatures from 750°C to 1000°C were chosen, as this allows for the thermal decomposition of calcite. This temperature range is also close to the documented outlet temperatures for the CentRec® receiver but below the ore's sintering temperature (1100°C to 1300°C). The control temperature is used to control the feed rate to the receiver reactor and does not determine the discharge temperature. The discharge temperature is a result of the energy balance.

Table II

Receiver model parameters (Ebert et al., 2016, 2018, 2019; Amsbeck et al., 2018)

Description	Value	Unit
Diameter, *D*	1.13	m
Length, *L*	1.695	m
Aperture, *A*	1	m^2
Particle layer thickness, d	20	mm
Void fraction, *v*	0.38	–
Drive power	7.5	kW
Rotational speed, max	80	rpm
Rotational speed, normal	45	rpm

In the HSC process model, the off-gas was treated as an infinite-volume tank that captured all process emissions. This approach allowed easy evaluation of the carbon dioxide produced by the process for a specific scenario. Similarly, the product pile was an infinite-volume container reporting each chemical species by weight. The full derivation of the view factor-based energy distribution model and its validation is given as (Hockaday, 2023).

The residence time of particles in the rotary receiver can be difficult to quantify (Gallo et al., 2016). The process model assumption in this study is that the rotary receiver may be described as a series of continuous stirred tank reactors (CSTR) in series. This assumption has implications for the particle residence time distribution in the reactor. Some particles may theoretically never leave the perfectly mixed reactors, while others rush through without reacting. The mean residence time for a reactor can always be calculated from the reactor mass holdup divided by the steady-state inlet or outlet mass flow rate. In this process model, the mean residence time, τ, represents the average time for a particle to move through the receiver reactor.

$$\tau = \frac{\text{mass holdup in reactor, kg}}{\text{material flow rate, kg/min}} \quad [1]$$

It may appear at first glance that the assumption of a well-mixed tank does not describe the behaviour of the rotary receiver. However, the receiver has a 10 mm high holding rim, damming part of the particle mass and preventing plug flow behaviour. In addition, particles in a rotary receiver are expected to behave or vibrate in all directions and change positions within the particle layer.

Methodology

The two ore samples used to construct the kinetic reaction rate models were also used as feed materials for the process evaluation. The measured compositions of the feed materials are given in Table III, with high braunite manganese ore abbreviated as braunite manganese (BMN) and high crypromelane manganese ore abbreviated as cryptomelane manganese (CMN)

Developing the heliostat field model for the solar plant

The performance of the solar plant was modeled to provide a dataset of hourly solar flux values that can serve as input to the dynamic HSC model. The methodology of modeling the solar thermal plant is based on the previously proposed methods (Amsbeck et al., 2014; Lubkoll, Hockaday and Harms, 2018). The solar thermal plant is based on the Centrec® receiver and heliostats of equivalent size to Heliopod® technology (Mckechnie, McGregor and Venter, 2022). The Centrec® receiver (i) is suitable for handling of solid material, so can be used for the pretreatment of manganese ore particles, (ii) it enables direct irradiation of the ore without the need to go via a heat transfer medium (this matches the experimental on-sun testing approach), (iii) has been extensively demonstrated at semi-commercial scale at the DLR's Juelich facility, and finally, (iv)

Table III

Composition of two manganese ore samples in wt.%

	High braunite Mn ore (BMN.)	High cryptomelane Mn ore (CMN.)
MnO^2	2.56	17.08
Mn_7SiO_{12}	41.74	27.02
Mn_2O_3	0.84	1.85
Mn_3O_4	7.19	7.87
SiO_2	3.42	6.21
Fe_2O_3	6.18	6.87
K_2O	0.05	1.10
Cr_2O_3	0.51	-
P_2O_5	0.06	0.07
$BaSO_4$	0.37	0.30
Na_2O	0.03	0.21
C	1.78	1.92
$CaMg(CO_3)_2$	17.61	-
$CaCO_3$	16.48	20.00
CaO	-	1.68
MgO	-	-
$Mn_2O_3.3H_2O$	0.09	0.72
Al_2O_3	-	-
$Al_2O_3.3H_2O$	1.09	0.98
$MgCO_3$	-	6.12

it can be scaled up to larger sizes understood by the solar thermal and mineral's processing industry. The Centrec® receiver operation and design are well documented (Amsbeck et al., 2018; Ebert et al., 2019) and may possibility be scaled further in the future (Gallo et al., 2016). This technology is being tested for commercialization in the HiFlex project (Santamarta, 2020; Sayles, 2020).

The design point for the solar thermal plant was taken as the DNI at midday on the solar equinox. The location assessed was the mining town of Hotazel in the Northern Cape province of South Africa. Hotazel is in the Kalahari Manganese Field, with large manganese mines belonging to different companies surrounding the town. The heliostat field design was done using SolarPILOT Version 1.3.2 software (Wagner, 2017, 2019) and is shown in Figure 2.

Table IV

Specifications for heliostats, receiver, and site

Specification	value	unit
Heliostat facet optical aperture area	1.83×1.22=2.23	m^2
Heliostat facet focal length	At slant	m
Receiver aperture	1	m^2
Receiver tilt angle	-45	°
Solar field design power	2.5	MW_t
Tower height	40	m
Site latitude (true)	-27.2	°N
Site longitude	22.9	°E
Design point DNI	1040	W/m^2
Solar field size	3760	m^2
Average solar field efficiency at the design point	62.6	%
Incident flux reaching the receiver	5503	MWh/a
Capacity factor (CF) based on incident flux	25	%

Hourly azimuth and elevation angles for the equinox, summer solstice, and winter solstice were calculated in Excel based on the equations for observer-sun angles (Stine and Geyer, 2011). These angles were then used in SolarPILOT as parametric input to determine the heliostat field efficiency curves. The output was interpolated to provide the heliostat field efficiency for each hour of the year. The land requirement for a 2.5 MW tower and solar field is approximately 160 m x 110 m or 1.76 ha.

Specifications for the SolarPILOT program are given in Table IV. Mirror performance parameters were set to 0.97 reflective surface ratio, 0.95 mirror reflectivity, and a soiling factor of 0.95. The receiver's horizontal acceptance angle was set to 80° and the vertical acceptance angle to 90°.

Results and discussions

The process model allowed for the investigation of a solar thermal process operation on different time scales. The residence time of the particles in the solar receiver, the temperatures in distinct parts of the receiver and the off-gas composition were estimated. Since the solar resource is variable, there is a concern that products from direct solar treatment may be erratic and inconsistent in quality.

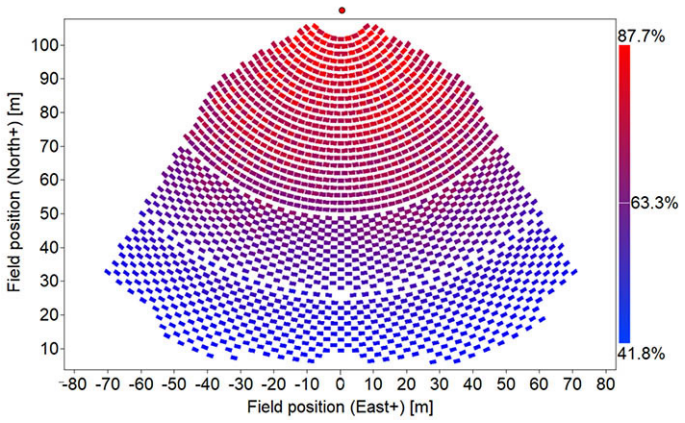

Figure 2—Heliostat field layout with total heliostat efficiency gradient displayed

This perception was investigated by running daily and monthly scenarios at the design specifications (ideal conditions) and non-ideal conditions (cloudy or rainy days). Due to the short residence time of the particles in the reactor, the simulations were done with 1-minute timesteps.

Product quality and throughput per day

A day with patchy sunshine was selected and modeled to compare the throughput and quality to a day of bright uninterrupted sunshine. January 18th was chosen from the typical meteorological year (TMY) as a high irradiance day, and June 26th as a day with interrupted sunshine. The hourly power to the receiver is shown in Figure 2. The BMN ore was used for illustrative purposes.

The operation of the pretreatment plant should consistently produce a product below 1200°C to prevent the melting or sintering of the particles. If the particles should sinter, they may destabilize the particle layer and initiate the dumping of the material. In addition, molten material may stick to the receiver walls and solidify, leading to solid material build-up that can prevent the free flow of the particles.

The extent of calcination is positively influenced by higher temperatures and negatively by higher feed rates. Higher feed rates reduce the residence time of the material in the receiver and increase untreated material that gets passed through to the product. Several simulations at different feed rates were run for the ores to investigate the operating window where the temperatures were below 1200°C, while the product achieved a calcination target of 80% or more for both the design case and the low solar irradiation case. A limit to the solar irradiance incident on the receiver was imposed to achieve the required calcination while maintaining a temperature below 1200°C. The limit of 1700 kW irradiance combined with the feed rate setpoint of 3200 kg/h reached the operational targets for the BMN ore, while the CMN ore had a feed rate setpoint of 6400 kg/h. The difference in feed rate is due to the different compositions of the ores, and the different reaction kinetics for the calcination of the ores. Due to the unreactive nature of the BMN ore compared to the CMN ore, the BMN ore simulations operated on feeding only when the discharge zone temperature was above 980°C. In contrast, the CMN ore achieved calcination above 80% even with feeding when the discharge zone temperature was 780°C.

The irradiance limit also has practical advantages. Since the solar field has extra design capacity it lengthens the steady-state operational time achieved daily. The solar multiple, defined as the solar plant design power divided by process energy demand, was 1.47 for this study.

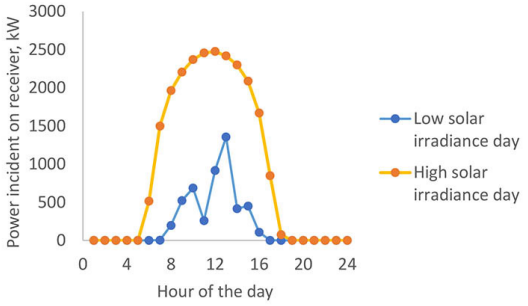

Figure 3—Power to the receiver on a high and low solar irradiance day

The BMN ore at a feed rate of 3200 kg/h illustrates how the receiver operates for a high solar irradiance day (the design case), and a low irradiance day (a deviation). The energy flows for the solar receiver are provided in Figure 3.

While zone temperatures fluctuated at sunrise and sunset, each tank operated at a constant temperature for most of a sunny day, as shown in Figure 4 (a). Figure 4 (b) shows temperatures are erratic for a cloudy day, fluctuating by 200°C to 300°C.

The extent of reactions is discussed next, based on the oxidation state and calcination degree of the material as it moves through the reactor.

The oxidation state of the manganese ore may be expressed as a non-stoichiometric compound, MnO_x, where x represents the amount of oxygen bound to manganese. For example, a highly oxidized ore would have a value of x close to 2, indicating that it contains mainly pyrolusite, MnO_2. A reduced hausmannite ore would have a value of x of 1.33 or 4/3 as it contains mainly Mn_3O_4. Similarly, one can express the amount of oxygen bound to Fe in the sample with FeO_y. Here, y will be equal to 1.5 for hematite, 1.33 for magnetite and 1 for wustite. For braunite, Mn_7SiO_{12}, we treat the oxygen to manganese ratio is treated to 10/7 or 1.43, and the remaining two oxygens are assumed to be bound to the silicon. The value of x reduces as thermal decomposition and reduction of manganese ores progress. The amount of organic carbon present in the feed material, the material's temperature, and the material's residence time in the high-temperature zone all limit the extent of reduction. During days with interrupted sunshine or low solar irradiance, more reduction may occur as feed rates are slower and residence times longer, as shown in Figure 6.

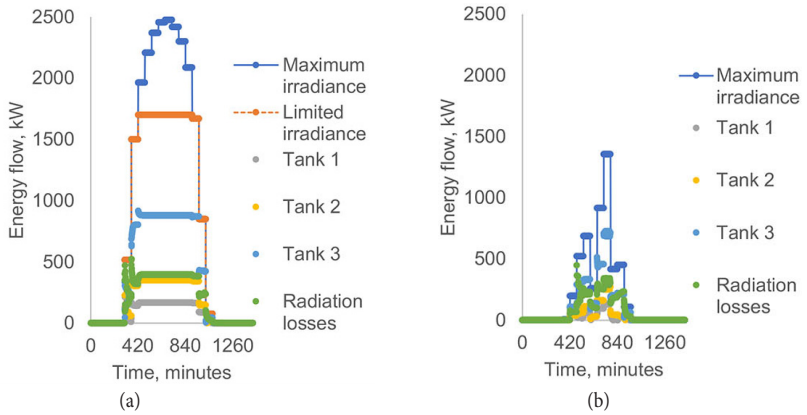

Figure 4—Energy flows for the solar receiver on an (a) high solar irradiance day and b) on a low solar irradiance day as calculated at a feed rate setpoint of 3200 kg/h BMN ore with a control temperature of 980 °C. At an irradiance of 1700 kW, radiation losses were 413 kW (24%). The kiln thermal efficiency, defined as the heat absorbed by the tanks over the incident power, was 76%

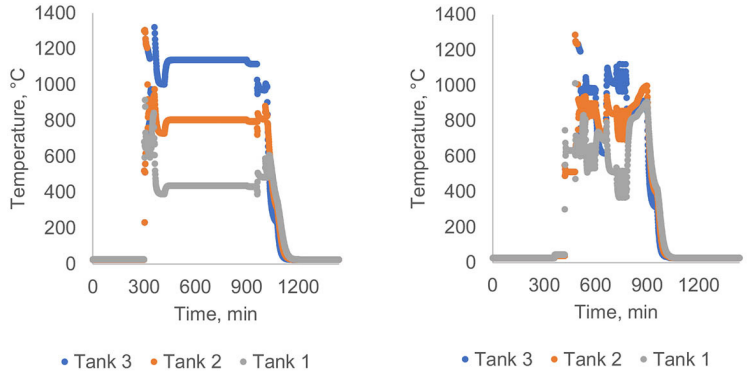

Figure 5—Temperatures for solar receiver zones on an (a) high solar irradiance day and (b) on a low solar irradiance day as calculated at a feed rate setpoint of 3200 kg/h BMN ore with a control temperature of 980°C

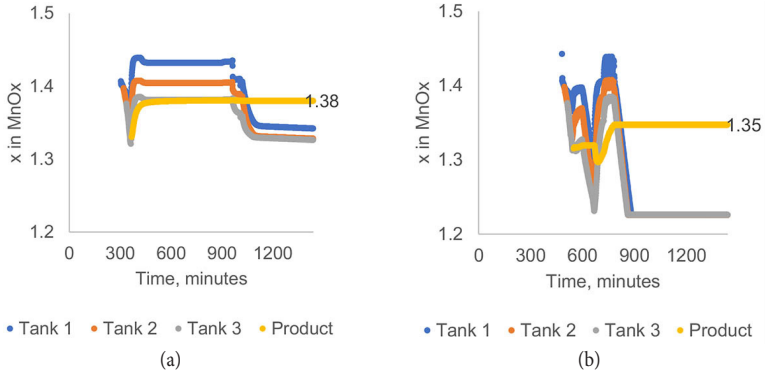

Figure 6—The value of x in MnOx in Tank 1, Tank 2, and Tank 3 and the product pile for an (a) high solar irradiance day and a (b) low solar irradiance day

The extent of calcination reactions achieved is presented in Figure 6. Calcination occurred when temperatures were above 700°C. The final product maintained a calcination degree of >80% due to the selection of a high control temperature (980°C) and halving of the feed rate when irradiance to the receiver was below 1000 kW. Calcination continued in the tanks after sunset while tank temperatures remained high enough. Variability in the product composition may be lessened by heat recovery from the product to preheat the feed, by using indirect solar heating with thermal storage (Hockaday et al., 2020), or by raising the solar multiple in the heliostat field design. These options all have implications for the cost of solar thermal treatment as more space and capital are needed for heat exchangers or heliostats. Another way to smooth variability in product quality would be to implement more sophisticated feed rate control or to set an irradiance limit below which material is not treated. These strategies incur no plant modifications but will reduce the production rate of the solar thermal pretreatment plant.

The evaluations showed that products of similar grade could be obtained for both high and low solar irradiance conditions. During periods of interrupted solar irradiance, the product may vary in the level of calcination and reduction due to variances in temperature and residence time. However, the quantities produced are small, reducing the overall effect on product quality.

Monthly and annual throughput of a solar pretreatment facility for manganese ores

The annual production of a solar thermal pretreatment plant was estimated by evaluating the summer and winter solstice months and an equinox month for each ore. The summer and winter solstice months' production was then multiplied by three and added to 6 times the equinox month's production, and this total was then divided by 369 and multiplied by 365 to scale to the number of days in a year.

Each scenario was analysed according to the product quality, measured by the extent of reduction and calcination achieved. The throughput and average product temperature were evaluated over one-minute timesteps. The results for each ore are given in Table V. Each scenario took about 2 hours to simulate and contains much more data (Hockaday, 2023) than can be displayed, so only summaries are provided here.

The composition of the products from solar thermal pretreatment is given in Table VI.

Table VI shows the mass reduction of the treated product compared to the untreated ore is 10.3% for the CMN ore and 11.9% for the BMN ore. This reduction in mass will translate directly to reduced transport costs as ores are usually moved by rail on a per-ton basis. Scope 1 CO_2 emissions were 0.09 t CO_2/t product for CMN ore and 0.16 t CO_2/t product for BMN ore. The emission factor specified for sinter production is 0.2 t CO_2/ t product.

The mean residence time was calculated as the material in the reactor divided by the feed rate setpoints.

For the CMN ore, a 20 mm particle layer led to 561 kg material in the reactor. For a feed rate of 3200 kg/h, the mean residence time was 10.5 minutes, and for 6400 kg/h, the mean residence time was 5.3 minutes. Note that the residence time in the high-temperature zone, Tank 3, was only a third of this residence time, hence means particles will remain in the high-temperature zone for 1.75 to 3.5 minutes during sunny operating conditions.

For the BMN ore, a 20 mm particle layer led to 577 kg material in the reactor. For a feed rate of 1600 kg/h, the mean residence time

Table V
Composition of solar pretreated manganese ores in wt.%

	High braunite Mn ore (BMN_s)	High cryptomelane Mn ore (CMN_s)
MnO_2	0.00	0.03
$Mn7SiO_{12}$	38.90	27.15
Mn_2O_3	0.00	0.91
Mn_3O_4	17.82	27.75
SiO_2	4.95	7.21
Fe_2O_3	4.74	6.29
K_2O	0.06	1.23
Cr_2O_3	0.59	0.00
P_2O_5	0.07	0.08
$BaSO_4$	0.43	0.33
Na_2O	0.03	0.23
C	1.70	1.92
$CaMg(CO_3)_2$	3.91	0.00
$CaCO_3$	3.66	9.45
CaO	13.75	9.06
MnO	2.57	1.84
Fe_3O_4	2.06	1.22
MgO	3.63	2.13
FeO	0.25	0.09
Fe	0.04	0.01
Al_2O_3	0.83	0.71
$MgCO_3$	0.00	2.36
Total	100.00	100.00

was 21.6 minutes, and for 3200 kg/h, the mean residence time was 10.8 minutes. Particles remained in the high-temperature zone for 3.6 to 7.2 minutes during high irradiance conditions. Given the two-feed rate setpoints depending on the solar irradiance to the reactor, the particles experience heating rates of 125°C/min to 500 °C/min

To achieve calcination rates above 80% for both ores, the BMN ore required much higher temperatures (above 1000°C) and lower feed rates than the CMN ore (around 800°C) due to the different reaction kinetics found for each ore. In future studies, the process model may be used to investigate the relationship between the chosen operating temperature, the throughput of materials, and the product composition in greater detail to maximize the reduction in greenhouse gas emissions and electrical energy demand.

This study treated the solar pretreatment of manganese ores as a simple one-unit process. The pretreatment could also be done as part of a more integrated and energy-optimized process, with carbon capture and sequestration or heat recovery being possible process improvements.

Downstream benefits of solar pretreated material

Since the most significant use of manganese ores is ferroalloy production, the possible impact of products from the solar thermal treatment of manganese ores was investigated on a high-carbon ferromanganese (HCFeMn) smelter. In South Africa, smelting is done in alternating-current submerged arc furnaces (AC SAF). Manganese ores are fed to the smelters with silica as flux and coal as reductant. The reductant requirement is determined by the amount of bonded oxygen that must be removed from the ore to reduce the iron and manganese to the metal, plus the carbon that reports to the alloy. The electricity demand is based on the latent energy required to heat all the materials to the smelting temperature and the net enthalpy demand from the reactions. This study considers the benefits of feeding pretreated material to the smelter at ambient temperatures. The benefits of feeding hot material is not evaluated and the solar pretreatment process is not coupled to the smelting process.

The stoichiometric carbon requirement for smelting is defined as the amount of carbon necessary to reduce all manganese to metallic manganese and all iron to metallic iron (the study does not consider the formation of carbides). Carbon reporting to the alloy is assumed dissolved rather than bound for modelling purposes. The specific energy requirement (SER) to produce a high-the carbon ferromanganese alloy (78% Mn, 7.5 %C remainder Fe) at 1300°C, slag at 1500°C and off-gas at 700°C, was estimated based on an HSC distribution model with carbon addition of twice the stoichiometric requirement in the smelting process shown in Figure 7. Silica flux was added to maintain the furnace basicity at 1.28 (Broekman and

Table VI

Monthly and annual production summaries for solar-pretreated carbonaceous ores

CMN ore	December	March	June	Annual estimate
Ore treated, t	1242	1004	961	12498
Product, t	1116	901	861	11212
Product, °C	818	818	823	819
t CO_{2eq}/t product	0.09	0.09	0.09	0.09
Off gas, t	693	670	649	7956
Off gas, °C	196	175	169	179
x in MnOx	1.37	1.37	1.37	1.37
% Calcined	86.5	86.6	87.0	86.7
BMN ore	**December**	**March**	**June**	**Annual estimate**
Ore treated, t	817	663	641	8265
Product, t	720	585	565	7281
Product, °C	1089	1092	1098	1093
t CO_{2eq}/t product	0.16	0.16	0.16	0.16
Off gas, t	686	663	642	7877
Off gas, °C	303	262	248	269
x in MnO*x*	1.38	1.38	1.38	1.38
% Calcined	82.7	82.6	82.7	82.7

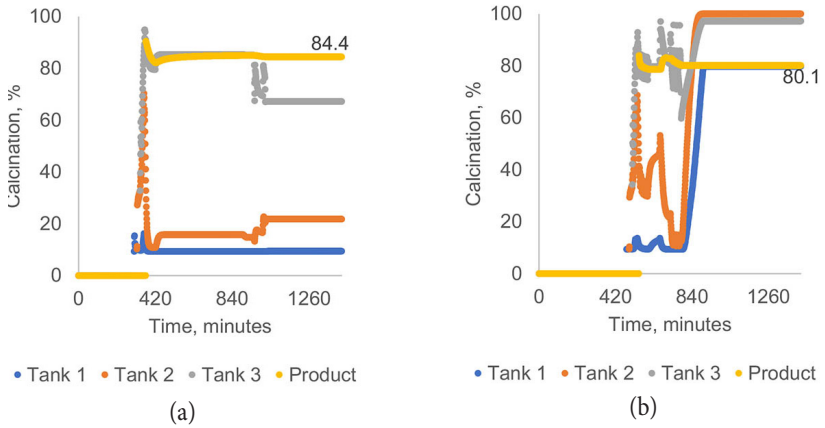

Figure 7—Calcination extent in Tank 1, Tank 2, Tank 3, and the product pile for an (a) high solar irradiance day and a (b) low solar irradiance day

Ford, 2004). The furnace off-gas was assumed to have a CO/CO_2 ratio of 70/30. CO_2 emissions were calculated based on the complete combustion of the furnace off-gas stream with air in a combustion chamber. The mass and energy balances were solved iteratively in the HSC Simulation module.

The annual production of pretreated material in a solar thermal plant with a 2.5 MW_t design point is summarized for the two ores in Table V. These materials, and the untreated ores, were considered inputs to the smelting process. The smelting characteristics of the treated materials were named for their ores with subscript 's' indicating solar thermal pretreatment.

The results for the smelting simulations for the BMN and CMN ores are given in Table VII.

Using solar-pretreated material lowers the SER per ton alloy produced by 38.7% for the BMNs ore compared to untreated BMN ore. Total CO_2 emissions per ton alloy are lowered by 19.3% for BMNs material compared to untreated ore. Solar pretreatment

Table VII

Smelting production, consumption and CO_2 emissions of BMN and CMN ores compared to solar pretreated ores (indicated by subscript s)

	BMN	BMNs	CMN	CMNs
Alloy production, (t alloy)/(t ore)	0.301	0.344	0.334	0.365
Carbon requirement, t/(t alloy)	0.820	0.685	0.844	0.631
Specific energy requirement, kWh/(t alloy)	1924	1180	1267	1258
Total CO_2 emissions, t/(t alloy)	5.090	4.107	4.386	3.814

reduces the SER per ton alloy produced by 0.6% for the CMNs ore compared to untreated CMN ore, and no significant reduction in electricity consumption was achieved by solar thermal pretreatment of the CMN ore. Compared to untreated ore, CO_2 emission per ton alloy is lowered by 13% for CMNs material.

The total CO_2 emissions were calculated to include the CO_2 emissions during the solar thermal pretreatment and CO_2 emissions from grid-connected electricity use, as shown in Figure 8. Scope 2 emissions from electricity consumption were determined from a grid electricity emission factor of 0.95 t CO_{2eq}/MWh (Takahashi and Louhisuo, 2022), and all electricity was assumed to be sourced from the national grid.

For a smelting operation that maintains production of 160 tons of metal per day (Broekman and Ford, 2004), the amount of treated ore required to replace untreated ore is roughly 170 000 tons annually for the BMN ore and 160 000 tons annually for the CMN ore. The annual production of a 2.5 MWt solar pretreatment plant is around 8000 tons/year for the BMN ore, therefore 21 of these plants will be required to meet this demand. The estimated footprint of such a solar pretreatment plant would be 37 ha. For the CMN ore, the annual production of a 2.5 MWt solar pretreatment plant is around 12 500 tons/year for BMN ore, hence, 13 of these plants will be required to meet this demand. The estimated footprint of such a solar pretreatment farm would be 23 ha. However, this can be built gradually as solar-pretreated material can be blended with untreated material to realize incremental benefits.

Financial modeling of levelized cost of heat from a solar plant

To evaluate the viability of using CST to directly pretreat manganese ores, it was necessary to estimate the cost of the energy provided and to compare it to alternative energy supplies. The CST plant process flow is shown in Figure 10.

The levelized cost of heat, LCOH_ST, can be described as the ratio of the discounted annual expenses over the discounted energy supplied (Short, Packey and Holt, 1995):

$$LCOH_{ST} = \frac{\sum_{n=0}^{n} \frac{C_n}{(1+r)^n}}{\sum_{n=0}^{n} \frac{Q_n}{(1+r)^n}}. \quad [1]$$

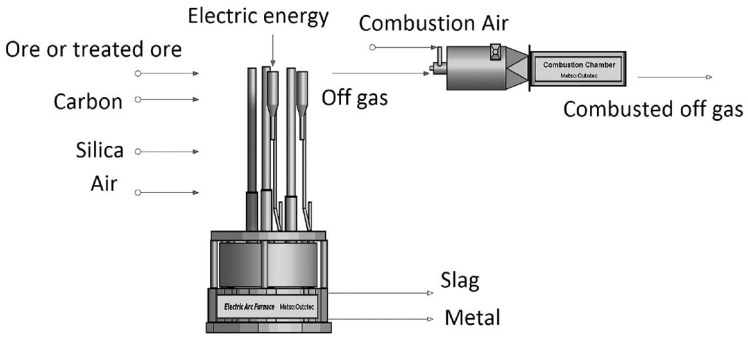

Figure 8—Schematic of high carbon ferromanganese smelter model

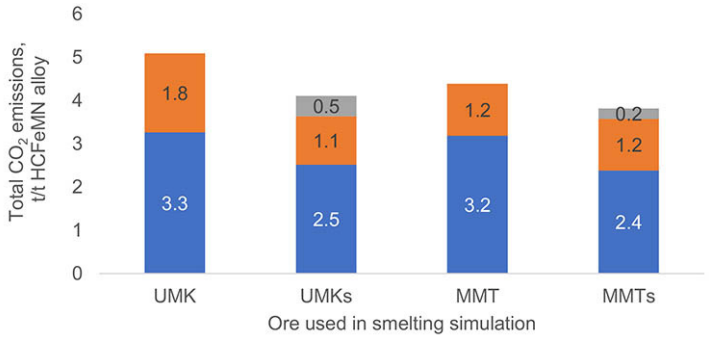

Figure 9—Breakdown of total CO_2 emissions calculation for scenarios comparing smelting of untreated ores with solar thermal pretreated ores

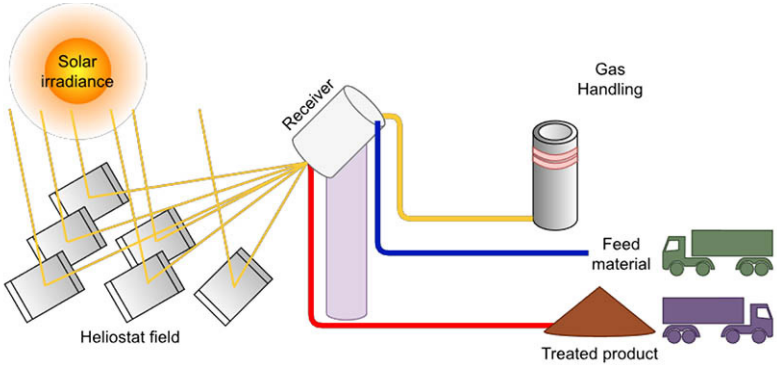

Figure 10—CST plant process illustrating components for LCOH capital expenditure

Table VIII

Cost assumptions for CAPEX of CST plant per 2.5 MWth tower

Item	Cost, R1000	Reference
Heliostat field @ 100 €/m²	7829	(Buck and Giuliano, 2019)
Receiver @ 123 k$	2204	(Lubkoll, Hockaday and Harms, 2018)
Vertical transport of feed materials (ores/reductant)	2249	(Lubkoll, Hockaday and Harms, 2018)
Tower	835	(Lubkoll, Hockaday and Harms, 2018)
Land cost (3500 R/ha)	6	(property24, 2022)
Total investment (Capital expenditure or CAPEX)	13123	

where n is the number of years in the lifetime of the project, C_n is the total expenses in year n and Q_n is the total amount of energy supplied in year n, and r is the discount rate considering the time value of money (or opportunity cost). The meaning of the $LCOH_{ST}$ is the price making the production of process energy break even at the end of the payback period. To be financially viable, one can compare the cost to alternatives and then show that the benefit (product produced) can make it worth doing.

The cost assumptions for the solar thermal process solution were based on a modular system consisting of a heliostat field surrounding a tower with a peak power delivery of 2.5 MWt. All costs were converted to South African rand (R) in the year of publication and adjusted for inflation to 2022. Inflation rates were found online (Inflationtool, 2022). Financial costs were converted back to USD at a conversion rate of R17.19/USD. It is estimated that the cost of undeveloped land in the Hotazel area is around USD204/ha based on advertised farms for sale (property24, 2022). In addition to the capital outlay described in Table VIII, operating and maintenance costs (O&M) are estimated at 3.9% of the CAPEX annually, and insurance costs at 1% of the CAPEX annually. Indirect costs are estimated at 22% of CAPEX annually

The levelized cost of heat from the solar thermal plant ($LCOH_{ST}$) was calculated over a project lifetime of 20 years, assuming the total investment is paid off over 20 years at a debt interest rate of 7%, as USD22/MWh. The plant produces a minimum of 8000 tons of treated ore BMN and 12 000 tons of treated CMN ore, making the cost of solar pretreatment USD5.6 per ton of BMN ore and USD4.0 per ton of treated CMN ore. The

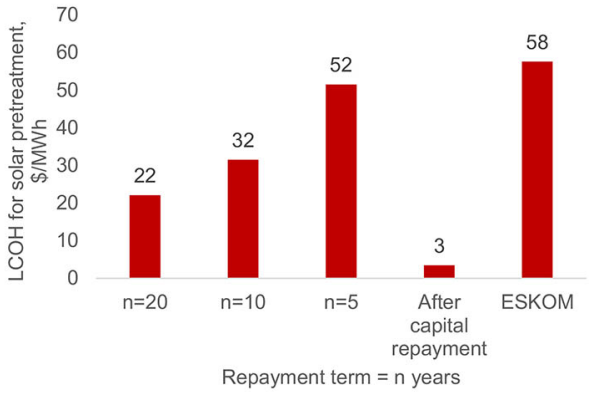

Figure 11—CST plant LCOHth for varying payback periods compared to average ESKOM grid electricity tariffs

cost of electricity, coke breeze and diesel costs for process heating were estimated to compare as alternative sources of process heat. Grid electricity cost in South Africa, which may be calculated from published tariffs by ESKOM (ESKOM, 2022), is a seasonally adjusted average of USD58/MWh without considering transmission network charges, distribution network charges or ancillary services. The change in LCOH for different repayment periods and the cost of solar thermal treatment after repayment of capital expenditure compared to the grid electricity cost in Soutth Africa is shown in Figure 11.

The diesel price in South Africa is R24.16/litre (Fuel SA, 2022) at the time of writing. Since diesel has an energy value of 11.83 kWh/kg (Boyle, 2012) and a density of 0.846 kg/litre (Engineering Toolbox, 2003), the cost of heating with diesel is USD140/MWh.

Between 2010 and 2020, the price of coal traded between USD50 per metric ton and USD130 per ton. Due to the volatility in the coal price, it is challenging to estimate its current and future costs. The cost of coal has increased sharply since 2020 and, during October 2022, was as high as USD400 per metric ton (IndexMundi, 2022; Trading Economics, 2022). Knowing that the cost of CST process heat is R380/MWh and coal has a calorific value of 8.39 kWh/kg, a parity cost of coal with CST process heat can be calculated as USD178.5 per ton.

It is therefore clear that concentrating solar thermal heating is cost competitive with other energy sources and in particular with electric or indirectly fire kilns. The benefits for ferromanganese smelters need to be evaluated based on the effect of changing from smelting untreated ore to pretreated ore. This study evaluates the benefits realized in reduced electricity consumption and reduced carbon monoxide emissions (as reduction in carbon tax).

The carbon tax liability was based on a full tax of USD8/ton of carbon dioxide emitted. Current legislation (South African Government, 2019) provides for industry allowances of 60% to 95% of total emissions at no cost, resulting in much lower liabilities in the short term. The intention is to gradually reduce emission allowances until the full tax (USD20/ton carbon dioxide) is applied. Replacing untreated ores with solar thermal treated ores may reduce future carbon tax liabilities, as shown in Figure 12.

The financial impact of including solar pretreated ores in high-carbon ferromanganese production is summarized in Table IX, assuming carbon tax liability of USD20/t CO_2 over both the smelter and the solar pretreatment plant. The electricity savings cover the cost of solar pretreatment of the BMN ore. The solar pretreatment of

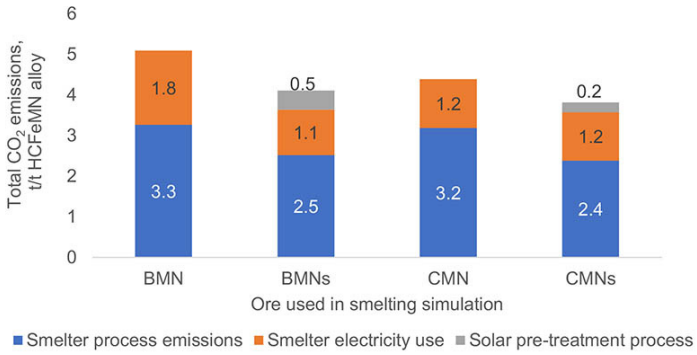

Figure 12—Total CO_{2eq} emissions for smelting untreated ore (BMN, CMN) compared to smelting pretreated ore (BMNs, CMNs)

Table IX

Financial impact of using solar pretreatment on HCFeMn production, based on $LCOH_{th}$ of \$22/MWh_{th} for CST plant

BMN ore treatment	BMNs	CMNs
Solar treatment cost, \$/(ton alloy)	(16)	(11)
Electricity savings, \$/(ton alloy)	43	0.5
Carbon tax savings, \$/(ton alloy)	8	5
Project savings, \$/(ton alloy)	**35**	**(6)**

the CMN ore cannot be offset by the electricity savings and possible carbon tax avoidance unless carbon tax liabilities double or the cost of solar thermal pretreatment halves. The savings in pretreating BMN ore, as shown in Table IX, amounts to USD2 million annually (assuming 160 ton/ day alloy production from BMNs ore).

Pretreatment of manganese ores with solar thermal energy may become an attractive project to avoid emissions and qualify for rebates, especially for braunite and calcite-rich ores. Such projects may also be eligible for certified emissions reductions tradable in the international carbon market.

Conclusions

This study investigated the solar thermal pretreatment of two carbonate-rich manganese ores and evaluated the performance of a rotating particle receiver to achieve 80% calcination of the ores. The solar thermal plant used typical meteorological year data and a heliostat field model to determine the hourly input of solar flux to the rotating receiver. A validated view factor-based energy distribution model was used to attribute the solar irradiance to three reactor zones and to determine radiation losses from the receiver. The products from the rotary solar receiver were based on reaction kinetics explicitly determined for each ore. It was found that the braunite-rich ore with a high activation energy of calcite decomposition benefits most from the solar thermal treatment, even though the high energy demand for calcination reduced the throughput of the solar thermal treatment plant.

The high braunite, calcite-rich ore (BMN) showed a reduced specific energy consumption for high carbon ferromanganese production of 39% and reduced CO_2 emissions of 19%. The high cryptomelane, and high calcite ore (CMN) showed reduced specific energy consumption of only 0.6% and reduced total CO_2 emissions of 13%.

Although the solar thermal treatment cost of the CMN ore is lower than for the BMN ore, the financial case for solar thermal treatment of the BMN ore is more favourable due to the electricity savings afforded by the solar thermal pretreatment. In contrast, the economic case for the solar thermal pretreatment of CMN ore is weak, as no significant reduction in electricity demand was realized.

The study shows that the benefit of concentrating solar thermal treatment (or other oxidative calcination processes) is highly dependent on the reaction kinetics of the materials to be treated. Two superficially similar ores in manganese and carbonate content may exhibit vastly different decomposition and reduction behaviour.

Acknowledgements

This paper is published with permission of Mintek. The authors would like to acknowledge Transalloys for providing the ore samples studied.

Credit author statement

SACH: Conceptualization, Methodology, Validation, Visualization, Original draft preparation, Funding
FD, QR, CM: Supervision, Review.

References

Amsbeck, L. 2014. 'Particle tower system with direct absorption centrifugal receiver for high temperature process heat', in *Energy Procedia 00 (2015) 000–000. SolarPACES 2014*, Beijing, China: Elsevier.

Amsbeck, L. 2018. First tests of a centrifugal particle receiver with a 1m² aperture, in *AIP Conference Proceedings. SolarPACES 2017: International Conference on Concentrating Solar Power and Chemical Energy Systems*, Santiago, Chile: AIP Publishing. Available at: https://doi.org/10.1063/1.5067040

Biswal, A. 2015. Electrolytic manganese dioxide (EMD): a perspective on worldwide production, reserves and its role in electrochemistry. *RSC Advances*, vol. 5, no. 72, pp. 58255–58283. Available at: https://doi.org/10.1039/C5RA05892A

Boyle, G. (ed.) 2012 *Renewable Energy, Power for a sustainable future*. Oxford University Press.

Broekman, B.R., Ford, K.J.R. 2004. The Development and Application of a HCFeMn Furnace Simulation Model for Assmang Ltd, in *Proceedings: Tenth International Ferroalloys Congress. INFACON X: 'Transformation through Technology'*, Cape Town, South Africa: SAIMM, pp. 194–205.

Buck, R., Giuliano, S. 2019. Solar tower system temperature range optimization for reduced LCOE, in. *SOLARPACES 2018: International Conference on Concentrating Solar Power and Chemical Energy Systems*, Casablanca, Morocco, p. 030010. Available at: https://doi.org/10.1063/1.5117522

Daavittila, J. 2001. Sintered Manganese Ore and Its Use in Ferromanganese Production, in *The Ninth International Ferroalloy Congress. INFACON IX*, Quebec City, Canada, pp. 212–222. Available at: https://www.pyrometallurgy.co.za/InfaconIX/212-Jorma.pdf

Ebert, M. 2016. Upscaling, Manufacturing and Test of a Centrifugal Particle Receiver, in *Volume 1: Biofuels, Hydrogen, Syngas, and Alternate Fuels; CHP and Hybrid Power and Energy Systems; Concentrating Solar Power; Energy Storage; Environmental, Economic, and Policy Considerations of Advanced Energy Systems; Geothermal, Ocean, and Emerging Energy Technologies; Photovoltaics; Posters; Solar Chemistry; Sustainable Building Energy Systems; Sustainable Infrastructure and Transportation; Thermodynamic Analysis of Energy Systems; Wind Energy Systems and Technologies. ASME 2016 10th International Conference on Energy Sustainability collocated with the ASME 2016 Power Conference and the ASME 2016 14th International Conference on Fuel Cell Science, Engineering and Technology*, Charlotte, North Carolina, USA: American Society of Mechanical Engineers, p. V001T04A007. Available at: https://doi.org/10.1115/ES2016-59252

Ebert, M. 2018. First On-Sun Tests of a Centrifugal Particle Receiver System, in *ASME 2018 12th International Conference on Energy Sustainability. ASME 2018 12th International Conference on Energy Sustainability collocated with the ASME 2018 Power Conference and the ASME 2018 Nuclear Forum*, Lake Buena Vista, Florida, USA: American Society of Mechanical Engineers, p. V001T11A002. Available at: https://doi.org/10.1115/ES2018-7166

Ebert, M. 2019. Operational experience of a centrifugal particle receiver prototype, in. *SOLARPACES 2018: International Conference on Concentrating Solar Power and Chemical Energy Systems*, Casablanca, Morocco, p. 030018. Available at: https://doi.org/10.1063/1.5117530

Ekman, B.M., Brooks, G., Rhamdhani, M.A. 2014. A Review: Solar Thermal Reactors for Materials Production', in C. Wang et al. (eds) *Energy Technology* 2014. Hoboken, NJ, USA: John Wiley & Sons, Inc., pp. 1–14. Available at: https://doi.org/10.1002/9781118888735.ch1

Engineering Toolbox 2003. *Fuels - Densities and Specific Volumes*. Available at: https://www.engineeringtoolbox.com/fuels-densities-specific-volumes-d_166.html (Accessed: 28 September 2022).

ESKOM. 2022. ESKOM *Schedule-of-standard-prices-2022_23*. Available at: https://www.eskom.co.za/distribution/wp-content/uploads/2022/03/Schedule-of-standard-prices-2022_23.pdf (Accessed: 28 September 2022).

Flamant, G. 2018. Solar processing of reactive particles up to 900°C, the SOLPART project, in. *SolarPACES 2017: International Conference on Concentrating Solar Power and Chemical Energy Systems*, Santiago, Chile, p. 020004. Available at: https://doi.org/10.1063/1.5067013

Fuel SA. 2022. *Fuel SA - South African Fuel - Petrol and Diesel Data*. Available at: https://www.fuelsa.co.za/#current (Accessed: 28 September 2022).

Gallo, A. 2016. Considerations for Using Solar Rotary Kilns for High Temperature Industrial Processes with and Without Thermal Storage, in *Proceedings of EuroSun2016. EuroSun2016*, Palma de Mallorca, Spain: International Solar Energy Society, pp. 1–10. Available at: https://doi.org/10.18086/eurosun.2016.02.04

Gasik, M. (ed.) 2013. *Handbook of ferroalloys: theory and technology*. Amsterdam: Elsevier/Butterworth-Heinemann.

Gericke, W.A. 1989. The establishment of a 500 000 t/a sinter plant at Samancor's Mamatwan mine', in *Proceedings of 5th International Ferroalloys Congress. Infacon V*, New Orleans, USA, pp. 24–33. Available at: https://www.pyrometallurgy.co.za/InfaconV/ (Accessed: 5 February 2020).

Gordon Y.N.J. 2013. Methods of manganese ore thermal-treatment prior to smelting- what to choose?, in *Efficient technologies in ferroalloy industry. The thirteenth International Ferroalloys Congress*, Almaty, Kazakhstan, pp. 05–16.

Gordon, Y., Nell, J., Yaroshenko, Y. 2018. Manganese Ore Thermal Treatment Prior to Smelting, *KnE Engineering*, vol. 3, no. 5, pp. 71–86. Available at: https://doi.org/10.18502/keg.v3i5.2656

Harris, K., Meyer, D.M., Auerswald. 1977. The production of electrolytic manganese in South Africa. *Journal of South African Institute of Mining and Metallurgy*, vol. 77, no. 7, pp. 137–149. Available at: https://hdl.handle.net/10520/AJA0038223X_738 (Accessed: 28 October 2020).

Hockaday, L. 2020. The Impact of Solar Resource Characteristics on Solar Thermal Pre-heating of Manganese Ores, in X. Chen et al. (eds). *Energy Technology 2020: Recycling, Carbon Dioxide Management, and Other Technologies*. Cham: Springer International Publishing (The Minerals, Metals & Materials Series), pp. 3–13. Available at: https://doi.org/10.1007/978-3-030-36830-2_1

Hockaday, L. 2021. A comparison of direct concentrating solar thermal treatment of manganese ores to fossil fuel based thermal treatments, in *Proceedings of INFACON XVI. International Ferro-alloys Congress*, Trondheim, Norway: SINTEF/NTNU/FFF. Available at: Not published, under review.

Hockaday, S.A.C. 2023. *Solar Thermal Treatment of Manganese Ores*. University of Stellenbosch.

Hockaday, S.A.C., Dinter, F., Harms, T.M. 2018. Introducing solar thermal heat into minerals processing: A case study on replacing a diesel burner at a sinter plant, in *Proceedings of South African Solar Energy Conference. SASEC 2018*, Durban: SASEC2018. Available at: https://www.sasec.org.za/full_papers/74.pdf (Accessed: 17 April 2019).

Hockaday, S.A.C., Dinter, F., Reynolds, Q.G. (In print) The thermal decomposition kinetics of carbonaceous and ferruginous manganese ores in atmospheric conditions, *Journal of Southern African Institute of Mining and Metallurgy* [Preprint].

IndexMundi. 2022. *Coal, South African export price - Monthly Price - Commodity Prices - Price Charts, Data, and News*. Available at: http://www.indexmundi.com/commodities/?commodity=coal-south-african (Accessed: 26 October 2022).

Inflationtool. 2022. *South Africa Inflation Rate - 2022*. Available at: https://www.inflationtool.com/rates/south-africa (Accessed: 28 September 2022).

International Resource Panel. 2020. *How minerals and metals companies can help achieve 2030 Agenda for Sustainable Development, UNEP*. Available at: http://www.unep.org/news-and-stories/story/how-minerals-and-metals-companies-can-help-achieve-2030-agenda-sustainable (Accessed: 17 January 2023).

Ishak, R., Tangstad, M. 2007. Degree of prereduction without coke consumption in industrial furnaces, in. *INFACON XI*, New Delhi, India: The Indian Ferro Alloy Producers' Association, pp. 268–279. Available at: https://www.pyrometallurgy.co.za/InfaconXI/ (Accessed: 16 November 2020).

Koepf, E. 2017. A review of high temperature solar driven reactor technology: 25years of experience in research and development at the Paul Scherrer Institute, *Applied Energy*, 188, pp. 620–651. Available at: https://doi.org/10.1016/j.apenergy.2016.11.088

Lubkoll, M., Hockaday, S.A.C., Harms, T.M. 2018. Integrating Solar Process Heat into Manganese Ore Pre-Heating', in. *SASEC 2018*, Durban, p. 8. Available at: https://www.sasec.org.za/full_papers/57.pdf (Accessed: 17 April 2019).

Malan, J., Barthel, W., Dippenaar, B.A. 2004. Optimizing manganese ore sinter plants: Process parameters and design implications, in *Proceedings: Tenth International Ferroalloys Congress. INFACON X*, Cape Town, South Africa: SAIMM, pp. 281–290. Available at: https://pyrometallurgy.co.za/InfaconX/057.pdf

Mckechnie, T., McGregor, C., Venter, G. 2020.Concentrating Solar Thermal Process Heat for Manganese Ferroalloy Production: Plant Modelling and Thermal Energy Storage Dispatch Optimization, in *ASME 2020 14th International Conference on Energy Sustainability. ASME 2020 14th International Conference on Energy Sustainability*, Virtual, Online: American Society of Mechanical Engineers, p. V001T14A001. Available at: https://doi.org/10.1115/ES2020-1635

Mckechnie, T., McGregor, C., Venter, G. 2022. Large HelioPodTM field layout design and optimisation, in. *SOLARPACES 2020: 26th International Conference on Concentrating Solar Power and Chemical Energy Systems*, Freiburg, Germany, p. 140008. Available at: https://doi.org/10.1063/5.0085721

Mills, R. 2021. ESG seen as biggest risk to mining industry, 13 April. Available at: https://aheadoftheherd.com/esg-seen-as-biggest-risk-to-mining-industry/ (Accessed: 17 January 2023).

Olsen, S.E., Tangstad, M., Lindstad, T. 2007. *Production of manganese ferroalloys*. Trondheim, Norway: Tapir Academic Press.

Outotec. 2019. *HSC Sim – Process Simulation Module.* Available at: https://www.outotec.com/products/digital-solutions/hsc-chemistry/hsc-sim-process-simulation-module/ (Accessed: 3 September 2019).

Pienaar, P.C., Smith, F.P. 1992. A Case Study of the Production of High-grade Manganese Sinter from Low-grade Mamatwan Manganese Ore, in *Proceedings of the 6th International Ferroalloys Congress*, Cape Town. INFACON 6, Johannesburg, South Africa: SAIMM, pp. 131–138. Available at: https://pyrometallurgy.co.za/InfaconVI/1131-Pienaar.pdf

Property24. 2022. *Farms for sale in Hotazel*. Available at: https://www.property24.com/farms-for-sale/hotazel/northern-cape/2533 (Accessed: 6 October 2022).

Purohit, S. 2018. Solar processing of composite iron ore pellets: Preliminary assessments', *Journal of Cleaner Production*, vol. 205, pp. 1017–1028. Available at: https://doi.org/10.1016/j.jclepro.2018.09.112

Roine, A., Bjorklund, P. 2002. *Outokumpu HSC Chemistry for Windows*. 02103-ORC-T. Finland: Outotec Research Oy.

Santamarta, J. 2020. EU HiFlex project - Concentrated solar power for sustainable pasta, *HELIOSCSP*, 14 October. Available at: https://helioscsp.com/eu-hiflex-project-concentrated-solar-power-for-sustainable-pasta/ (Accessed: 6 January 2023).

Sayles, R. 2020. *Solar tower at pasta plant spurs new generator design | Reuters Events | Renewables, Reuters Events | Renewables.* Available at: https://www.reutersevents.com/renewables/solar-thermal/solar-tower-pasta-plant-spurs-new-generator-design (Accessed: 6 January 2023).

Short, W., Packey, D.J., Holt, T. 1995. *A manual for the economic evaluation of energy efficiency and renewable energy technologies.* Manual NREL/TP--462-5173, 35391. Golden, Colorado: NREL, p. NREL/TP--462-5173, 35391. Available at: https://doi.org/10.2172/35391

South African Government. 2019. *Carbon Tax Act 15 of 2019*. Available at: https://www.gov.za/documents/carbon-tax-act-15-2019-english-afrikaans-23-may-2019-0000 (Accessed: 2 September 2019).

Stine, W.B., Geyer, M. 2011. *Power From The Sun*. Available at: https://www.powerfromthesun.net/ (Accessed: 10 February 2021).

Takahashi, K., Louhisuo, M. 2022. IGES List of Grid Emission Factors. Institute for Global Environmental Strategies. Available at: https://doi.org/10.57405/iges-1215

Tanabe, I. 1968. Preheating of Ore for a Ferromanganese Furnace-a Recent Trend in Japan. *Journal of Metals*, vol. 20, pp. 81–87. Available at: https://doi.org/10.1007/BF03378711

Tangstad, M., Ichihara, K., Ringdalen, E. 2015. Pretreatment Unit in Ferromanganese Production, in *The Fourteenth International Ferroalloys Congress. INFACON XIV*, Kiev, Ukraine: INFACON, p. 8. Available at: https://www.pyrometallurgy.co.za/InfaconXIV/099-Tangstad.pdf (Accessed: 4 October 2019).

Trading Economics. 2022. *Coal - 2022 Data - 2008-2021 Historical - 2023 Forecast - Price - Quote - Chart*. Available at: https://tradingeconomics.com/commodity/coal (Accessed: 26 October 2022).

Wagner, M.J. 2017. *Optimization of stored energy dispatch for concentrating solar power systems*. PhD. Colorado School of Mines. Available at: https://hdl.handle.net/11124/171000.

Wagner, M.J. 2019. *Solar Power Tower Integrated Layout and Optimization Tool | Concentrating Solar Power | NREL*. Available at: https://www.nrel.gov/csp/solarpilot.html (Accessed: 3 September 2019).

Zhang, H. 2013. The Mechanism on Biomass Reduction of Low-Grade Manganese Dioxide Ore, *Metallurgical and Materials Transactions B*, vol. 44, no. 4, pp. 889–896. Available at: https://doi.org/10.1007/s11663-013-9835-7. ◆